Mach-Zehnder Interferometer-based Integrated Terahertz Temperature Sensor

Youqiao Ma, Nghia Nguyen-Huu, Jun Zhou, Hiroshi Maeda, Qiang Wu, Mohamed Eldlio, Jaromír Pištora and Michael Cada

***Abstract*: A plasmonic Mach-Zehnder interferometer (MZI) for temperature sensing is reported in the terahertz (THz) regime. The MZI is formed by embedding a semiconductor (SC) layer into a silicon membrane, where the SC layer supports two independent propagating surface plasmon polariton (SPP) waves on both surfaces. The temperature-sensitive phase difference between these two SPP waves gives rise to the modulation of the transmitted intensity. The results show that the MZI sensor possesses a sensitivity and a Figure of Merit (FoM) as high as 8.9 × 10^{-3} THz/K and 117, respectively. Theoretical calculations indicate that the further improvement in sensing performance is still possible through optimization of the structure. Moreover, an investigation of structural perturbations indicates that the MZI has a good tolerance to the fabrication errors. The compact MZI-based waveguide structure may find important applications in areas of sensing and integrated THz circuits.**

***Index Terms*: Terahertz, Plasmonics, Mach-Zehnder interferometers, Temperature sensors**

I. Introduction

As a promising candidate for the next-generation on-chip biosensing technology, surface plasmon polariton (SPP) is attracting significant research interest [1]. SPP is the electromagnetic (EM) waves coupled to electron oscillations and propagating along the interface between a metal and a dielectric. SPP, characterized by the maximum field distributed at the metal surface, can be extremely sensitive to the changes of the local dielectric properties, such as those induced by the surface molecular binding events [2]. Because of this remarkable property, SPP has become a basic standard for the detection of label-free and real-time biochemical reactions [3].

A typical SPP biosensing system employs a prism to couple the incident EM waves into the SPP, which is well known as the Kretschmann configuration [4]. This approach offers relatively high sensitivities. However, the bulky structure makes it difficult for realization of on-chip integration. On the other hand, nanoplasmonic biosensors, such as nanostructured metal films and nanoparticles, are emerging sensing platforms that can overcome the above limitation and are therefore becoming potential alternatives to the conventional SPP sensors [5-8]. The nanostructured SPP sensors can have small footprints, down to a few square micrometers, making them easily integrated on a chip with microfluidics [9]. However, their sensing capability is generally limited by the relatively low sensitivity, broad spectral linewidth and weak resonance intensity [10-11]. The reported refractive index (RI) sensitivities (detection limits) for these nanoplasmonic sensors are one to two orders of magnitude lower (larger) than those of typical prism-based sensing systems [12-13]. Another widely used nanoplasmonic sensing technique is SPP interferometry, which uses the phase-sensitive interference to control the linewidth of the interference pattern, which may improve the sensing resolution [14-16]. Numerous interferometer-based SPP biosensors have been proposed and experimentally investigated recently, such as slit-groove structures [14-15], slit-slit structures [16] and slit-grating structures [17].

Most efforts have been spent developing plasmonic sensors within the optical frequency [4-17]. The terahertz (THz) frequency, on the other hand, is attracting more and more attention from biological researchers because numerous characteristic vibrational modes of the bio-molecules, such as proteins and DNA, exist in the THz spectrum [18]. Furthermore, the properties of the THz waves are highly dependent on the water content, suggesting that there are ways to characterize the water content in sample materials by using the THz spectroscopy [19]. However, the SPP modes supported by a metal-dielectric interface at THz frequencies are loosely confined, because they are far below the plasma frequency of metal [20]. An alternative material to support the low-frequency SPP is the doped semiconductor, which provides a more versatile method to engineer the propagation properties of SPP than metals [21]. In this regard, several semiconductor-based THz plasmonic sensors have been studied [22-24]. One of those is the stub-cavity-based SPP (SCSPP) sensors, whose high-compact size was reported on recently [22-23]. Due to the large loss of the cavity mode, this type of sensor suffers from a wide spectral linewidth [24]. To address

This work was supported by Applied Science in Photonics and Innovative Research in Engineering (ASPIRE), a grant supported by the Natural Sciences and Engineering Council's (NSERC) Collaborative Research and Training Experience (CREATE) program of Canada, the Grand Agency of Czech Republic (#15-21547S), and the National Natural Science Foundation of China (Grant nos. 61320106014 and 61275153).

Y. Q. Ma, N. N. Huu, M. Eldlio and M. Cada are with Dalhousie University, Halifax, B3J 3L3 Canada (e-mail: mayouqiao188@hotmail.com, nghianano@gmail.com, meldlio@dal.ca, and michael.cada@dal.ca).

J. Zhou is working at Ningbo University, Zhejiang, 315211 China (e-mail: zhoujun@nbu.edu.cn).

H. Maeda is with Fukuoka Institute of Technology, Fukuoka, 811029 Japan (e-mail: hiroshi@fit.ac.jp).

Q. Wu is with Northumbria University, Newcastle, NE18ST United Kingdom (e-mail: qiang.wu@northumbria.ac.uk).

J. Pištora is with Technical University of Ostrava, Ostrava-Poruba, 70833 Czech Republic (e-mail: jaromir.pistora@vsb.cz).

this issue, a novel silicon-on-insulator (SOI)-based semiconductor sensing configuration was recently proposed [25]. It is designed to exhibit a maximum SPP absorption at a certain temperature within the frequency of interest. The location of the absorption valley is sensitive to the changes of the surrounding temperature with a sensitivity of 7.5 × 10^{-3} THz/K. More importantly, the fabrication process of such a structure is simple and complementary metal-oxide-semiconductor (CMOS) compatible [26].

In this work, we would like to point out that the sensing scheme in [25] could be realized using another novel method, i.e. the Mach-Zehnder (MZ) interferometry. The interferometric sensor consists of a semiconductor layer embedded in a silicon membrane. The interference between the two SPP waves, propagating along both surfaces of a semiconductor layer, causes a modulation in the transmitted intensity. The temperature-dependent transmission patterns make the structure useful as a temperature sensor. Investigation of temperature sensors is very important because the temperature is a fundamental factor in many processes ranging from industrial engineering to life sciences.

This paper is organized as follows: In Section II, the basic considerations and design principle are introduced. An analytical interference model is also developed to predict the THz response. In Section III, the modal and transmission characteristics are studied using the Finite Element Method (FEM). A temperature sensor is investigated based on the optimized structural parameters and it achieves a sensitivity (Figure of merit) as high as 8.9 × 10^{-3} THz/K (117). Finally, the conclusions are discussed in Section IV.

II. Basic Considerations and Design Principle

A schematic sketch of the proposed Mach-Zehnder interferometer-based (MZI) THz sensor is shown in Fig. 1. All the structural characteristics and coordinating systems are also depicted in the figure. The refractive indices of silicon (Si) and silica (SiO_2) are almost temperature (frequency) independent within a temperature (frequency) range from 270 K (0.5 THz) to 310 K (10 THz) [27, 28]; thus their refractive indices are considered as constants of $n_{Si} = 3.4$ and $n_{sio_2} = 1.95$ in the present work [27, 28]. The losses of Si and SiO_2 are not taken into account, because their extinction coefficients are negligible within frequency of interest [29-31]. Moreover, the indium antimonide (InSb) is selected as the semiconductor material due to its narrow energy gap and large electron density, which has been demonstrated to support the low-loss and tight-confined THz SPP modes [32]. The permittivity of InSb (ε_{InSb}) is described by the Drude model [33]

$$\varepsilon_{InSb} = \varepsilon_\infty - \frac{Ne^2}{\varepsilon_0 m_{eff}} \frac{1}{\omega(\omega+i\gamma)} = \varepsilon_\infty + \frac{Ne^2}{\varepsilon_0 m_{eff}\gamma\omega} \frac{i}{(1-i\frac{\omega}{\gamma})} \quad (1)$$

where $\varepsilon_\infty$is the high-frequency permittivity, ε_0 is the vacuum permittivity, ω is the angular frequency, γ is the damping constant, e is the electron charge, m_{eff} is the effective mass of a free carrier, and N is the temperature-dependent intrinsic carrier density which can be written as [33]

$$N\ (m^{-3}) = 5.76 \times 10^{20} T^{1.5} \exp(-\frac{0.13}{k_B T}) \quad (2)$$

where T and k_B are the operating temperature and Boltzmann constant, respectively. In the very high frequency regime (i.e. $\omega/\gamma \gg 1$), Eq. 1 can be written approximately as

$$\varepsilon_{InSb} = \varepsilon_\infty - \frac{Ne^2}{\varepsilon_0 m_{eff}\omega^2} \quad (3)$$

As can be seen from Eq. 3, the term of $1/\omega^2$ becomes very small for very high frequencies, indicating that the distribution of carrier density in Eq. 3 can be neglected. Using this approximation, Eq. 3 can be simplified as $\varepsilon_{InSb} = \varepsilon_\infty$. Thus at high frequencies, the behavior of InSb is like that for a dielectric. On the other hand, in the very low frequency regime (i.e. $\omega/\gamma \ll 1$), Eq. 1 is approximate to

$$\varepsilon_{InSb} = \varepsilon_\infty + \frac{Ne^2 i}{\varepsilon_0 m_{eff}\gamma\omega} \quad (4)$$

According to Eq. 4, the effect of carrier density on ε_{InSb} becomes more important at very low frequencies. The large carrier density gives rise to the large real/imaginary part of refractive index, which makes the EM waves hardly penetrate into the material of InSb. In this regard, the SPP wave does not exist on a planar InSb-dielectric interface at low frequencies, or in other words, the material of InSb becomes the perfect conductor. Therefore, the electromagnetic properties of InSb are like those of metals at very low frequencies, while it exhibits a dielectric-like behavior at very high frequencies. A characteristic frequency at which the electromagnetic response of InSb changes from a dielectric to a metal is called the plasma frequency, i.e. $\omega_P = \sqrt{Ne^2/(\varepsilon_0 m_{eff})}$. The carrier density N depends strongly on the temperature T, which makes the plasma frequency $\omega_P$tunable by changing the temperature T. In the following calculations, the adopted parameters of the Drude model for InSb are set as ε_∞ = 15.68, m_{eff} = 0.015 m_e (where m_e is the mass of electron) and γ = 0.1π THz [34].

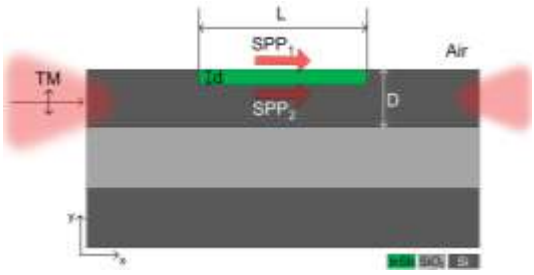

Fig. 1. Schematic diagram of proposed MZI-based THz temperature sensor. Two separated propagating SPP waves are supported on both surfaces of InSb layer.

Figure 2 (a) shows the real part of the permittivity of InSb (Re(ε_{InSb})) as functions of the operating temperature (T) and frequency of incident wave (f). It can be found that the value of Re(ε_{InSb}) is affected by the variation of T. With certain values of T and f, InSb can act as a plasmonic material because the requirement for Re(ε_{InSb}) < 0 is satisfied. Fig. 2 (b) depicts the dispersion relations for SPP on a single air-InSb interface with different T. From it, one can see that the SPP dispersion curves

deviate from the air light line, indicating that the InSb is capable of confining the EM waves on its surface, which is similar to the SPP modes for metals at optical frequency range. The SPP mode is loosely bound for a small value of β, but becomes more tightly bound as β increases. What's more, the SPP dispersions are influenced by the choice of the temperature, suggesting great promise for developing InSb-involved temperature-tunable devices.

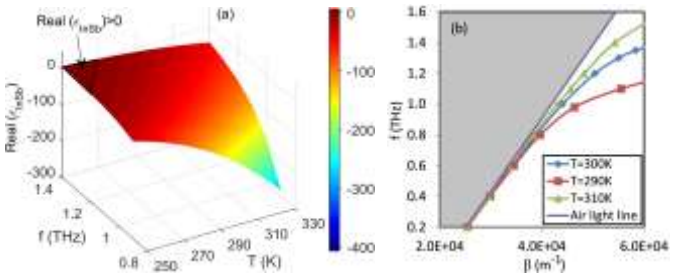

Fig. 2. (a) Three dimensional (3D) plot of real part of permittivity of InSb versus both temperature T and frequency f. Black line region shown in Fig. 2 (a) is a case of Real (ε_{InSb}) > 0. (b) Dispersion relations for SPP existing on a single air-InSb interface with different temperature T.

Assuming the waveguide is illuminated by a transverse-magnetic (TM) polarized light via the end-fire coupling scheme [35], then in principle, the two propagating SPP waves (SPP_1 and SPP_2) will be sustained on the upper and lower surfaces of the InSb layer, i.e. the air/InSb interface (sensing arm) and the Si/InSb interface (reference arm) [36]. The high refractive index difference between the air and Si results in a mismatched wave-vector between SPP_1 and SPP_2 waves, or in other words, the SPP_1 and SPP_2 waves will not couple with each other and propagate independently. When both SPP waves reach at the end of the InSb layer, they will interfere with each other and couple into the Si waveguide layer, depending on their relative phase difference ($\Delta\phi$). The total transmitted intensity I can be given by

$$I \propto \cos(\Delta\phi) = \cos[L(k_{SPP_2} - k_{SPP_1}] \qquad (4)$$

where L is the length of the sensing arm, and $k_{SPP_1}(k_{SPP_2})$ is the wavevector of the SPP_1 (SPP_2) wave which can be written as

$$k_{SPP_1} = k_0\sqrt{\frac{\varepsilon_{InSb}}{\varepsilon_{InSb}+1}}, k_{SPP_2} = k_0\sqrt{\frac{\varepsilon_{InSb}{n_{Si}}^2}{\varepsilon_{InSb}+{n_{Si}}^2}}, \qquad (5)$$

where k_0 is the propagation constant in free space. According to eq. (4), the constructive (destructive) interference of two SPP waves will take place when the value of $\Delta\phi$ equals to even (odd) multiples of π. In this way, one can obtain the constructive (destructive) resonance frequency f as

$$f = \frac{mc}{2L\left(\sqrt{\frac{\varepsilon_{InSb}{n_{Si}}^2}{\varepsilon_{InSb}+{n_{Si}}^2}} - \sqrt{\frac{\varepsilon_{InSb}}{\varepsilon_{InSb}+1}}\right)} \qquad (6)$$

where c is the free-space light speed, and m is the even (odd) integer. It is evident that the resonance frequency will change with the variations of T, which provides the basis of the proposed sensing scheme.

III. Results and Discussion

In the following, the modal properties and transmission were analyzed using the finite element method-based (FEM) software package (COMSOL Multiphysics) with the Radio Frequency (RF) module. A perfectly matched layer (PML) was employed at the calculation boundaries to absorb the reflection of the outgoing EM waves. Convergence tests were also done to assure the meshing and boundaries do not affect the solutions.

To function as a good interferometer, both arms of the MZI should be single mode waveguides, which is different from that in [25], where the structure was designed as a multimode waveguide (mode orders m = 0, 1 are supported). It is evident that the sensing arm supports one SPP_1 mode only. For the reference arm, the number of the supported mode is determined by the layer thickness D. To find the critical value of D for the single mode operation, Fig. 3 (a) shows the dependence of the real parts of effective mode indices for all guided modes with parameter D and frequency f. In this simulation, the other parameters are selected as follows: d = 5 μm, n_s = 1 and T = 300 K. As shown in Fig. 3 (a), the SPP_2 modes exist for all values of D considered in this plot, while for the fundamental waveguide (FWG) modes, they cannot be supported while D is smaller than 43 μm (58 μm) at frequency of 1.4 THz (1 THz), where their effective refractive indices are smaller than that of SiO_2, indicating the substrate leakage takes place.

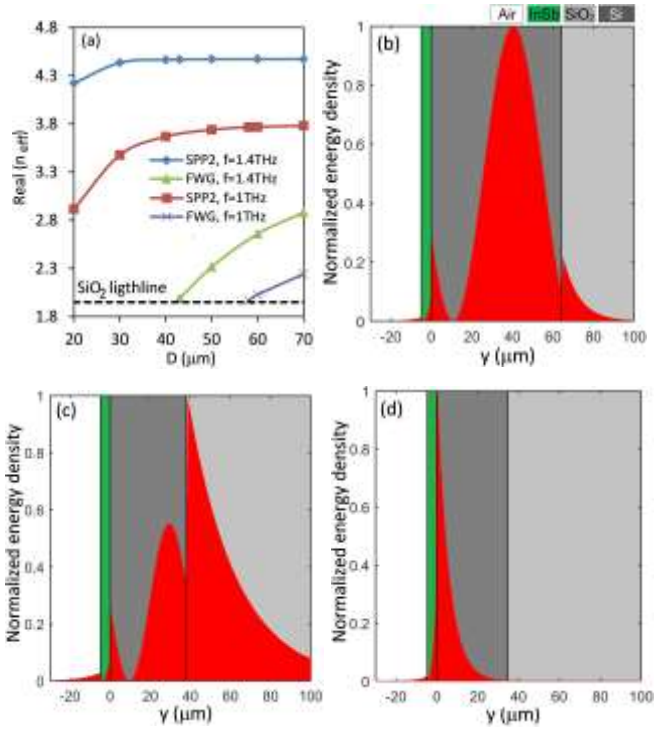

Fig. 3. (a) Real parts of effective refractive indices for all supported modes versus diameter D with different frequency f. Dotted line represents refractive index of SiO_2. Normalized energy density distributions for (b) FWG mode with [D, f] = [70 μm, 1.4 THz], (c) FWG mode with [D, f] = [43 μm, 1.4 THz] and (d) SPP_2 mode with [D, f] = [40 μm, 1.4 THz].

The normalized energy density distributions for the FWG modes at frequency of 1.4 THz with D = 70 μm and D = 43 μm are shown in Fig. 3 (b) and (c), respectively. Clearly, the energy of the FWG mode starts to radiate into the silica for the waveguide with D ≤ 43 μm. Therefore, in the following study, the value of D is fixed at 40 μm to ensure the reference arm behaving as a single mode waveguide. Fig. 3 (d) also depicts the normalized energy density distribution for the SPP_2 mode with f = 1.4 THz and D = 40 μm. It is shown that a negligible part of energy is located on the sensing arm, indicating that the phase property of the SPP_2 wave is not sensitive to any surrounding refractive index change. On the other hand, the field of SPP_2 mode distributed inside the InSb provides a very effective overlap between SPP_2 and InSb (whose permittivity is temperature-dependent), which potentially influents the temperature sensitivity.

The results in Fig. 4 (a) show the normalized transmission spectra with different length L. The parameters are chosen as D = 40 μm, d = 5 μm, n_s = 1 and T = 300 K for calculations. The obvious spectral oscillations are observed, and the transmitted intensity becomes smaller as L increases because of the increased propagation loss. The interference pattern exhibits a faster oscillation with the increase of L leading to the decreased valley linewidth. For example, the full width at half maximum (FWHM) for L = 1500 μm at f = 1.065 THz is 0.011 THz (~ 2.8 um), which is two times smaller than that for L = 1000 μm at f = 1.073 THz with FWHM = 0.025 THz (~ 6.5 um). This is physically reasonable because the interference period P is inversely proportional to the length L, i.e. $P \propto \lambda^2/L$ [16]. Moreover, through the further observation in Fig. 4 (a), one can find that the interference contrast ratio between the maximum and minimum transmissions increases as frequency f decreases. This is due to the propagation loss of SPP wave decreasing as frequency f decreases, which results in the stronger interference, resulting in a larger transmission contrast. Fig. 4 (b) depicts the relationship between the frequency f and integer m based on the analytical model developed above with L = 1000 μm (Eq. (6)). The predicted spectral positions of the peaks (where m are the even integers) agree very well with the FEM- simulated results, which validates our hypothesis that the oscillation patterns of transmission are the result of the interference between SPP_1 and SPP_2 waves.

To illustrate the feasibility of our sensing scheme, a temperature sensor was studied, as the phase difference between SPP_1 and SPP_2 waves is temperature-sensitive, or in other words, when SPP_1 and SPP_2 waves arrive in (out of) phase at the end of the InSb layer, the constructive (destructive) interference gives rise to the maximal (minimal) transmission. It is important to investigate this because the temperature sensors are the key components of any process-heating application because they provide temperature feedback about the process [37].

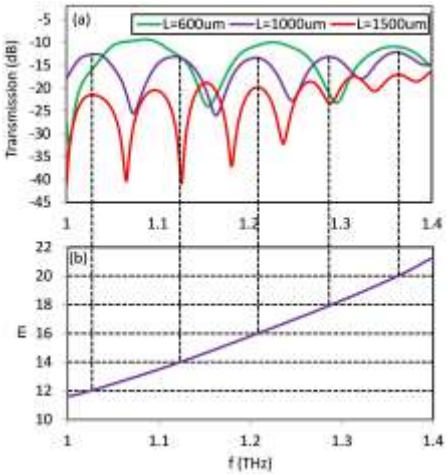

Fig. 4. (a) Normalized transmission spectra of MZI for the different value of L. (b) Relationship between integer m and frequency f obtained from Eq. 5 with L = 1000 μm.

Fig. 5 (a) depicts the normalized transmission spectra for different temperatures of T with D = 40 μm, d = 5 μm, n_s = 1 and L = 1000 um. As can be seen, the dip shifts toward a larger frequency as T increases, indicating that the variations of temperature can be monitored by measuring the shift of the valley frequency. The estimated sensitivity is 8.9×10^{-3} THz/K, which are comparable to that of 7.5×10^{-3} THz/K achieved in [25], but six times improved than that reported in [23] (1.425×10^{-3} THz/K). The structure offers an improved sensing performance. However, the frequency gap between two neighboring valleys is narrow (the frequency gap is 0.075 THz for T = 296 K), which limits the frequency range that can be monitored without the valley overlap. For example, within the frequency range of 0.075 THz, as T increases from 296 K to 305 K, the valleys starts to overlap (as marked by the dotted ellipse in Fig. 5 (a)). One effective way to overcome this limitation is to enlarge the interference period by decreasing the length L. Therefore, Fig. 5 (b) shows the normalized transmission spectra with L = 300 um. As expected, the range of detecting temperature is two times (from 290 K to 310 K) widened compared to the device with L = 1000 um (from 296 K to 305 K). Interestingly, this widened detecting range is achieved without sacrificing the sensitivity, which is estimated as 8.3×10^{-3} THz/K.

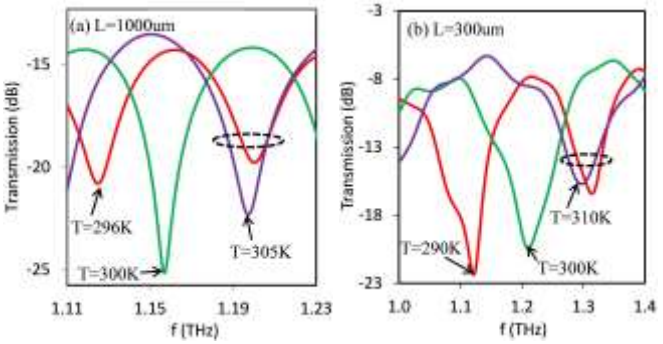

Fig. 5. Normalized transmission spectra of MZI-based temperature sensor for (a) L = 1000 um and (b) L = 300 um. The dotted ellipses indicate the overlap of valleys.

Another widely used key factor to evaluate the sensing performance is the Figure-of-Merit (FoM), which is defined as the ratio between the sensitivity S and FWHM, i.e. ($S \times T$)/FWHM. The sensitivities for structures with L = 300 um and L = 1000 um are comparable. However, the FoM for case of L = 1000 um (FoM = 117, with f = 1.156 THz and T = 300 K) is four times that of L = 300 um (FoM = 29, with f = 1.213 THz and T = 300 K). The result suggests that the FoM can be further enhanced by extending the length L, but the transmitted intensity will get lower, as shown in Fig. 4 (a).

Note that the structure is compatible with the CMOS technique. The suggested fabrication steps of the proposed structure are schematically shown in Fig. 6, which involve: (1) Deposition of a PMMA layer on a SOI substrate; (2) The groove could be formed by the electron-beam lithography (EBL) technique; (3) Deposition of InSb film with the ratio frequency magnetron sputtering technique [38]; (4) The PMMA layer could be dissolved in acetone and complete the proposed structure. However, a certain level of fabrication error is inherent in the process, i.e. the error of the etching depth h (as shown in the inset of Fig. 7 (a)). Thus, the discussion about the fabrication tolerance is highly desired. 7 (a) shows the variation of the sensitivity S as well as FoM versus h. In this simulation, the parameters are D = 40 μm, d = 5 μm, n_s = 1 and L = 1000 μm. It can be found that both values of S and FoM decrease when h increases. However, the decrease is modest. For example, if the value of h changes within 1 μm, the sensitivity S and FoM experience less than 0.5% and 8% variations, respectively. Particularly, the variation of the sensitivity S is as small as 1%, even when h equals to 2 μm. In addition, an alternative interferometer could be realized by lying the InSb film on top of the Si substrate, as shown in the inset of Fig. 7 (b) with $t = d$ = 5 μm. From it one can see that the influence of shift t on the sensing performance is insignificant. Such small variations of S on h (t) are because the propagation properties of SPP_1 and SPP_2 waves are slightly affected by the change of h (t). The simulation results confirm that the structure has a very good tolerance to the fabrication errors.

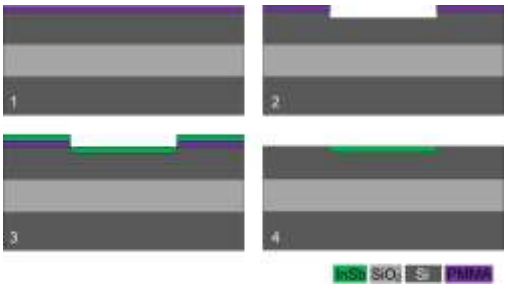

Fig. 6. Schematic diagrams of suggested fabrication steps.

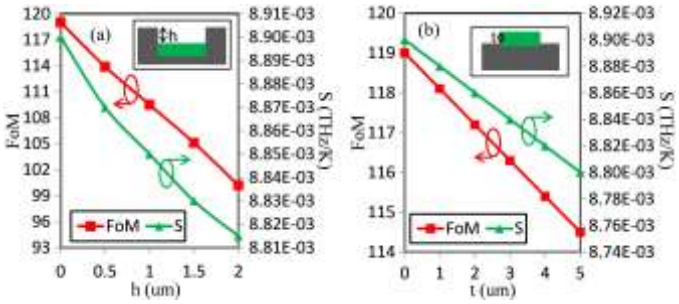

Fig. 7. (a) Influence of error of etching depth h on sensitivity S and FoM. Inset: schematic view of error of etching depth. (b) Influence of shift t on sensitivity S and FoM. Inset: schematic view of shift t.

On the basis of the above discussions, one can find that the sensing performance is highly affected by the sensing length L; therefore, carefully selecting the value of L is crucial. The choice of L should be made to balance the sensitivity, the interference period, the transmitted intensity and the FoM. For example, the narrow interference period and high FoM are preferred for biosensing applications, due to the small refractive index variation [39]. On the other hand, the proposed interferometry structure is foreseen to open new horizons in developing the electro-/thermo-THz modulators [40]. For example, THz modulation can be achieved via the free carrier plasma dispersion effect, in which a change in carrier density is used to change the refractive index of the semiconductor, which in turn modifies the propagation velocity of THz and the absorption coefficient.

IV. Conclusions

In conclusion, we have proposed and investigated a plasmonic MZI-based temperature sensor, which consists of a semiconductor layer embedded in a silicon membrane. Two propagating SPP waves are supported on both surfaces of the semiconductor layer, and their phase difference is influenced by the surrounding temperature. As a result, the field amplitudes of the two SPP waves interfere with each other, resulting in a modulation in the transmitted intensity. A theoretical interference model was also developed to predict the THz response, and it was validated by the FEM simulation. With the optimized parameters, the sensitivity and FoM could reach up to 8.9 × 10^{-3} THz/K and 117, respectively. We also demonstrated that the MZI sensor has a good tolerance to the fabrication errors. The enhanced sensing performance makes this compact device promising for integrated THz sensing platforms.

V. References

[1] A. G. Brolo, “Plasmonic for future biosensors,” Nat. Photon., vol. 6, pp. 709-713, 2012.

[2] N. Zhang, Y. J. Liu, J. Yang, X. D. Su, J. Deng, C. C. Chum, M. H. Hong, and J. H. Teng, “Highly sensitivity molecule detection by plasmonic nanoantennas with selective binding at electromagnetic hotspots,” Nanoscale, vol. 6, pp. 1416-1422, 2014.

[3] J. Homola, "Surface plasmon resonance sensors for detection of chemical and biological species," Chem. Rev., vol. 108, pp. 462-493, 2008.

[4] S. A. Maier, "Plasmonics: fundamental and applications," Springer: New York, 2007.

[5] M. E. Stewart, C. R. Anderton, L. B. Thompson, J. Maria, S. K. Gray, J. A. Rogers, and R. G. Nuzzo, "Nanostructured plasmonic sensors," Chem. Rev., vol. 108, pp. 494-521, 2008.

[6] Y. Wang, W. Knoll, and J. Dostalek, "Bacterial pathogen surface plasmon resonance biosensor advanced by long range surface plasmons and magnetic nanoparticle assays," Anal. Chem., vol. 84, pp. 8345-8350, 2012.

[7] C. Y. Tsai, K. H. Chang, C. Y. Wu, and P. T. Lee, "The aspect ratio effect on plasmonic properties and biosensing of bonding mode in gold elliptical nanoring arrays," Opt. Express, vol. 21, pp. 14090-14096, 2013.

[8] C. A. Barrios, V. Canalejas-Tejero, S. Herranz, M. C. Moreno-Bondi, M. Avella-Oliver, R. Puchades, A. Maquieira, "Aluminum nanohole arrays fabricated on polycarbonate for compact disc-based label-free optical biosensing," Plasmonics, vol. 9, pp. 645-649, 2014.

[9] A. D. Leebeeck, L. K. S. Kumar, V. D. Lange, D. Sinton, R. Gordon, and A. G. Brolo, "On-chip surface-based detection with nanohole arrays," Anal. Chem., vol. 79, pp. 4094-4100, 2007.

[10] K. M. Mayer, and J. H. Hafner, "Localized surface plasmon resonance sensors," Chem. Rev., vol. 111, pp. 3828-3857, 2011.

[11] A. M. Otte, B. Sepulveda, W. Ni, J. P. Juste, L. M. Liz-Marzan, and L. M. Lechuga, "Identification of the optimal spectral region for plasmonic and nanoplasmonic sensing," ACS Nano, vol. 4, pp. 349-357, 2010.

[12] Y. K. Gao, Q. Q. Gan, Z. M. Xin, X. H. Cheng, and F. J. Bartoli, "Plasmonic Mach-Zehnder interferometer for ultrasensitive on-chip biosensing," ACS Nano, vol. 5, pp. 9836-9844, 2011.

[13] A. Barik, L. M. Otto, D. Yoo, J. Jose, T. W. Johnson, and S. H. Oh, "Dielectrophoresis-enhanced plasmonic sensing with gold nanohole arrays," Nano Lett., vol. 14, pp. 2006-2012, 2014.

[14] Y. K. Gao, Z. M. Xin, Q. Q. Gan, X. H. Cheng, and F. J. Bartoli, "Plasmonic interferometer for label-free multiplexed sensing," Opt. Express, vol. 21, pp. 5859-5871, 2013.

[15] J. Feng, V. S. Siu, A. Roelke, V. Mehta, S. Y. Rhieu, G. T. R. Palmore, and D. Pacifici, "Nanoscale plasmonic interferometers for multispectral, high-throughput biochemical sensing," Nano Lett., vol. 12, pp. 602-609, 2012.

[16] Y. J. Wang, J. J. Chen, C. W. Sun, K. X. Rong, H. Y. Li, and Q. H. Gong, "An ultrahigh-contrast and broadband on-chip refractive index sensor based on a surface-plasmon-polariton interferometer," Analyst, vol. 140, pp. 7263-7270, 2015.

[17] X. W. Li, Q. F. Tan, B. F. Bai, and G. F. Jin, "Non-spectroscopic refractometric nanosensor based on a titled slit-groove plasmonic interferometer," Opt. Express, vol. 19, pp. 20691-20703, 2011.

[18] M. Nagel, M. Forst, and H. Kurz, "THz biosensing devices: fundamental and technology," J. Phys.: Condens. Matter., vol. 18, pp. S601-S618, 2006.

[19] E. C. Camus, M. Palomar, and A. A. Covarrubias, "Leaf water dynamics of Arabidopsis thaliana monitored in-vivo using terahertz time-domain spectroscopy," Sci. Rep., vol. 3, pp. 2910 (1-5), 2013.

[20] J. G. Rivas, "Terahertz: the art of confinement," Nat. Photon., vol. 2, pp. 137-138, 2008.

[21] M. Tonouchi, "Cutting-edge terahertz technology," Nat. Photon., vol.1, pp. 97-105, 2007.

[22] S. Ranjana, P. Bhatt, H. Surdi, B. R. Sangala, M. N. Satyanarayan, G. Umesh, and S. S. Prabhu, "Bio-interfacing of resonant transmission characteristics of InSb-based terahertz plasmonic waveguide," Biomed. Phys. Eng. Express, vol. 1, pp. 025003, 2015.

[23] H. Q. Liu, G. B. Ren, Y. X. Gao, Y. D. Lian, Y. Qi, and S. S. Jian, "Tunable subwavelength terahertz plasmon-induced transparency in the InSb slot waveguide side-coupled with two stub resonators," Appl. Opt., vol. 54, pp. 3918-3924, 2015.

[24] Y. Q. Ma, G. Farrell, Y. Semenova, and Q. Wu, "Analysis and applciations of nanocavity structures used as tunable filters and sensors," Infrered Phys. Techn, vol. 55, pp. 389-394, 2012.

[25] J. Shibayama, K. Shimizu, J. J. Yamauchi, and H. Nakano, "Surface plasmon resonance waveguide sensor in the terahertz regime," J. Lightwave Technol., vol. 34, pp. 2518-2525, 2016.

[26] A. V. Krasavin, and A. V. Zayats, "Photonic signal processing on electronic scales: electro-optical field-effect nanoplasmonic modulator," Phys. Rev. Lett., vol. 109, pp. 053901, 2012.

[27] C. Ronne, L. Thrane, P. Astrand, A. Wallqvist, K. V. Mikkelsen, and S. R. Keiding, "Investigation of the temperature dependence of dielectric relaxation in liquid water by THz reflection spectroscopy and molecular dynamic simulation," J. Chem. Phys., vol. 107, pp. 5319-5331, 1997.

[28] H. Iwao, "Optical thin film technology used in the terahertz frequency," J. Natl. Inst. Of Inf. Commun. Tech., vol. 51, pp. 87-94, 2004.

[29] J. M Dai, J. Q. Zhang, W. L. Zhang, and D. Grischkowshy, "Terahertz time-domain spectroscopy characterization of the far-infrared absorption and index of refraction of high-resistivity, float-zone silicon," J. Opt. Soc. Am. B, vol. 21, pp. 1379-1386, 2004.

[30] R. H. Giles, "Characterization of Material Properties at Terahertz Frequencies," Report, University of Massachusetts, Lowell, Submillimeter Technology Laboratory, 1995.

[31] http://www.tydexoptics.com/pdf/THz_Materials.pdf.

[32] X. Y. He, "Comparison of the waveguide properties of gap surface plasmon in the terahertz region and visible spectra," J. Opt. A: Pure Appl. Opt., vol. 11, pp. 045708, 2009.

[33] M. S. Dresselhaus, "Solid state physics part II: Optical properties of solids," Academic Press, New York, 1966.

[34] X. Y. Dai, Y. J. Xiang, S. C. Wen, and H. Y. He, "Thermally tunable and omnidirectional terahertz photonic bandgap in the one-dimensional photonic crystals containing semiconductor InSb," J. Appl. Phys., vol. 109, pp. 053104, 2011.
[35] J. P. B. Mueller, K. Leosson, and F. Capasso, "Polarization-selective coupling to long-range surface plasmon polariton waveguides," Nano Lett., vol. 14, pp. 5524-5527, 2014.
[36] S. Sidorenko, and O. J. F. Martin, "Resonant tunneling of surface plasmon polaritons," Opt. Express, vol. 15, pp. 6380-6388, 2007.
[37] M. A. Herrero, J. M .Kremsner, and C. O. Kappe, "Nonthermal microwave effects revisited: on the importance of internal temperature monitoring and agitation in microwave chemistry," J. Org. Chem., vol. 73, pp. 36-47, 2008.
[38] D. Y. Li, H. T. Li, H. H. Sun and L. C. Zhao, "Characterization of ultrathin InSb nanocrystals film deposited on SiO2/Si substrate," Nanoscale Res. Lett., vol. 6, pp. 601, 2011.
[39] A. Shalabney, and I. Abdulhalim, "Figure-of-merit enhancement of surface plasmon resonance sensors in the spectral interrogation," Opt. Lett., vol. 37, pp. 1175-1177, 2012.
[40] M. Rahm, J. S. Li, and W. J. Padilla, "THz wave modulators: a brief review on different modulation techniques," J Infrared Millim Terahertz Waves, vol. 34, pp. 1-27, 2013.

Youqiao Ma received the M. Sc. degree from the Faculty of Science, Ningbo University, Zhejiang, China, in 2010. In 2015, he received his PhD degree from Dublin Institute of Technology, Ireland. Currently he is working as a research fellow at Applied Science in Photonics and Innovative Research in Engineering (ASPIRE) in Dalhousie University, Canada. He has been involved in four national and international projects including Fiosraigh Science Foundation Ireland (TIDA), the Open Fund of the State Key Laboratory of Information Photonics and Optical Communications, and the Natural Sciences and Engineering Research Council of Canada (NSERC). He is authored more than 30 scientific papers and 10 conference proceeding papers. His research interests include fiber optics, plasmonic waveguides, terahertz devices, semiconductors, biosensing and energy-harvesting solutions.

Nghia Nguyen-Huu received the Bachelor's degree in mechanical engineering from the Can Tho University, Can Tho, Vietnam, in 2004, the dual Master's degree in mechanical engineering from the Institute National des Sciences Appliquees de Lyon, Villeurbanne, France, and Universitat Politecnica de Catalunya Barcelona, Barcelona, Spain, in 2007, and the Ph.D. degree from the Institute of Nanotechnology and Microsystems Engineering and the Department of Materials Science and Engineering, National Cheng Kung University (NCKU), Tainan, Taiwan, in 2012. He has authored ten SCI journals and some SPIE and IEEE conference proceedings. In addition, he has been an active Member of the Optical Society of America and SPIE, and reviews many high impact journals. He also serves as a Member of editorial boards of the journal, News in Engineering and International Journal of Microwave and Optical Technology. He is the recipient of some awards, including Postdoctoral Fellowships, 2014 SPIE Photonics Europe Travel Award, the First Place Best Poster Award at the 2011 International Symposium on Nano Science and Technology, Ph.D. Fellowship of NSRRC and NCKU from 2008 to 2012, Ph.D. Fellowship of Ministry of Education of Taiwan (declined), and Erasmus Mundus Scholarship of the Education and Culture of European Commission from 2005 to 2007. He has research interests in designing and optimizing nanophotonic structures for color filters, polarizers, energy harvesting systems, and biosensors. The design is mainly based on the physical mechanisms: Rayleigh Wood anomaly, surface plasmon polaritons, magnetic polaritons, and Fabry-Perot like phenomenon; and the numerical algorithms used as the rigorous-coupled wave method, finite-difference time-domain method, and a genetic algorithm. His research interests include the field of micro/nanoscale heat and fluid transport.

Jun Zhou received the B.Sc. degree in physics from the Anhui University of Science and Technology, Anhui, China, in 1982, and the M.Sc. and Ph.D. degrees in optics from Shanghai Jiaotong University, Shanghai, China, in 1990 and 1996, respectively. From 1999 to 2000, he was a Senior Researcher with the Photonics Laboratory, City University of Hong Kong, Hong Kong. From 2001 to 2002, he was a Research Fellow with the Institute of Cybernetics, Council of National Research, Pozzuoli, Italy. From 2002 to 2004, he was a Senior Research Fellow with the Institute of Microelectronics, Singapore. From 2005 to 2006, he was a Senior Visiting Scholar with the Applied Physics Laboratory, University of Washington, Seattle, DC, USA. He is currently a Professor with the Department of Physics, Ningbo University, Ningbo, China. He has authored 145 papers in international technical journals and conferences and contributed to a book chapter. His current research interests include the design and fabrication of optical circuits, photonic bandgap devices, optical sensor and SERS biosensors.

Hiroshi Maeda was born in Fukuoka, Japan, in July 1966. He received the B.E. degree in electronics engineering, M.E. degree in information systems engineering and D.E. degree in computer science and communication engineering from Kyushu University in 1989, 1991, and 1996, respectively. In 1997, he joined to Department of Information and Communication Engineering in Fukuoka Institute of Technology, Japan. His research interest is experimental approach for electromagnetic band gap structure. He also studies numerical analysis technique for wave-guiding structure and nonlinear optics. Prof. Maeda is a member of Optical Society of America (OSA), Institute of Electronics, Information and Communication Engineers (IEICE) Japan and Japan Society of Applied Physics (JSAP).

Qiang Wu received the B.S. degree in physics from Beijing Normal University, Beijing, China and the Ph.D. degree in fiber optics from the Beijing University of Posts & Telecommunications, Beijing, in 1996 and 2004, respectively. He was a Senior Research Associate with the Optoelectronics Research Centre, City University of Hong Kong, from 2004 to 2006, where he was involved in research on polymer optical waveguides. He was a Research Associate with the Applied Optics and Photonics Group, Heriot-Watt University, from 2006 to 2008, where he was involved in research on laser joining in micromanufacturing. He was a Stokes Lecturer with the Photonics Research Centre, Dublin Institute of Technology, from 2008 to 2015. He is currently a Senior Lecturer with Department of Mathematics, Physics & Electrical Engineering, Northumbria University, Newcastle Upon Tyne, NE1 8ST, United Kingdom. His current research interests include the design and fabrication of fiber Bragg grating devices and their applications for sensing, optical fiber interferometers for novel fiber optical couplers and sensors, nanofiber, microsphere sensors for bio-chemical sensing, and surface plasmon resonant. Dr. Wu has over 170 publications in the area of photonics.

Mohamed Eldlio received the B. Sc. degree from Academy of Aeronautic Studies and Sciences from Libya on 1983 and M .Sc. degree in electrical and computer engineering from Warsaw University of Technology, Faculty of Electronics and Information Technology-POLAND on 2002. He is currently a PhD candidate at electrical and computer engineering department at Dalhousie university. He is authored 10 journal papers and conference proceeding papers. His current research interests include surface plasmon polariton, hybrid waveguide, THz plasmonic, THz semiconductor plasmonic, photonics and biosensors.

Jaromír Pištora received the M.Sc. degree in theory of electromagnetic field from Czech Technical University, Prague, Czech Republic, in 1977, and the Ph.D. degree in experimental physics from Charles University, Prague, in 1984. He is currently a Professor of applied physics at VSB Technical University of Ostrava, Ostrava, Czech Republic, and the Director of Nanotechnology Center. He has published more than 300 papers in international journals and conference proceedings including 12 invited talks. He is a Member of the Optical Society of America, SPIE-Czech Chapter, Czech and Slovak Society for Photonics, Union of Czech Mathematicians and Physicists, EOS-Czech Chapter. He was a Visiting Professor at Kyushu University (1999, 2001), Research Institute of Electronics, Shizuoka University (2002, 2005–2006), and Dalhousie University (2007). He has also been the Chairman of the International Symposium on Microwave and Optical Technology (ISMOT), Ostrava 2003, and the vice-chairman of ISMOT 2005, Fukuoka, Japan. His research interests include magneto-optics, periodical structures, and magnetic sensors.

Michael Cada received the degree in electrical engineering from the Czech Technical University, Prague, Czech Republic, in 1976, and received the Ph.D. degree in technical sciences from the Czechoslovak Academy of Sciences, Prague, in 1979. Since his graduation, he has worked as a Research Associate with A.M. Prokchorov in Moscow, as an Assistant Professor at the Czech Technical University, as a Research Fellow at the Polytechnic University of New York, as a Visiting Researcher at NRC, as a Research Engineer at MPB in Montreal, as an Invited Professor at Ecole Polytechnique Federale in Lausanne, Switzerland, as an Industrial Fellow at BNR, and as a Guest Scientist at Siemens in Germany. He has attracted more than C$10 million in research funds; published more than 250 refereed articles, conference papers, and industrial reports; supervised more than 200 highly qualified personnel and set up a high-tech company. He is a Principal Investigator in a European Union nanotechnology training project that has recently attracted more than C$2 million in funding. He is also a Director of Natural Sciences and Engineering Research Council of Canada, Collaborative Research and Training Experience Program, and Applied Science in Photonics and Innovative Research in Engineering.